ACS OMEGA

http://pubs.acs.org/journal/acsodf

Article

Multiwalled Carbon Nanotube-Based On-Body Patch Antenna for Detecting COVID-19-Affected Lungs

Raja Rashidul Hasan,[‖] Ahmed Mortuza Saleque,[‖] Afrin Binte Anwar, Md. Abdur Rahman, and Yuen Hong Tsang*

Cite This: *ACS Omega* 2022, 7, 28265−28274

Read Online

ACCESS | Metrics & More | Article Recommendations | Supporting Information

ABSTRACT: A novel rectangular patch antenna based on multiwall carbon nanotubes has been designed and developed for assisting the initial detection of COVID-19-affected lungs. Due to their highly conductive nature, each nanotube echoes electromagnetic waves in a unique manner, influencing the increase in bandwidth. The proposed antenna operates at 6.63, 7.291, 7.29, and 7.22 GHz with a higher bandwidth classified as an ultrawide band and can be used on a human body phantom model because of its flexibility and decreased radiation qualities. Flame retardant 4 is chosen as a substrate with a uniform thickness of 1.62 mm due to its inexpensive cost and excellent electrical properties. The maximum specific absorption rate of the proposed antenna is obtained as 1.77 W/kg for 10 g of tissues. For testing purposes, a model including all the known features of COVID-19-affected lungs is developed. The designed antenna exhibits excellent performance in free space, normal lungs, and affected lung environments. It might be utilized as a first screening device for COVID-19 patients, especially in resource-constrained areas where traditional medical equipment such as X-ray and computerized tomography scans are scarce.

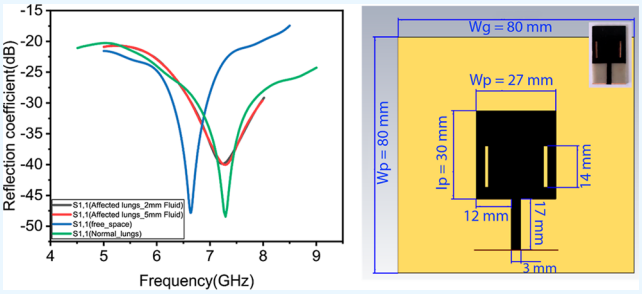

INTRODUCTION

The catastrophe from COVID-19 continues to rise throughout the world, causing fatal outcomes for patients of higher age and pre-existing chronic health conditions. Recent studies revealed that pneumonia caused by the novel coronavirus SARS-CoV-2 leads to pulmonary infection and causes respiratory failure, which is the underlying cause of the fatal outcome.[1,2] COVID-19 pneumonia tends to spread in both lungs. Air sacs in the lungs fill with fluid, limiting their ability to take in oxygen and causing shortness of breath, cough, and other symptoms. The lungs become filled with fluid and inflamed, leading to breathing difficulties, and the patient often requires high flow oxygen or even ventilator assistance. However, the early detection of COVID-19 pneumonia is crucial for proper intervention, thereby avoiding fatal outcomes.[3,4] Besides the mass vaccination program, early-stage detection and appropriate intervention are the suggested strategies to reduce the public health risk associated with this global pandemic. Though the reverse transcription polymerase chain reaction (RT-PCR) test can detect the presence of the novel coronavirus SARS-CoV-2 in the human body, it is unable to provide information about COVID-19 pneumonia or lung damage. Therefore, computerized tomography (CT) scan and X-ray results are the only way to diagnose COVID-19 pneumonia. Nevertheless, CT scans and X-ray machines are expensive and inaccessible in many resource-constrained regions. Even the developed countries struggle to handle the growing number of patients with their existing CT scan and X-ray facilities.[5] Therefore, there is a pressing need for cost-effective, handheld, accurate, and quicker diagnosis equipment for detecting COVID-19 pneumonia. There is considerable medical evidence linking affected lungs to the early detection of COVID-19. Xu et al. reported that chest CT scan images may be utilized for early detection of COVID-19.[6] In addition, Zu et al. revealed that typical chest CT scan images include peripherally distributed multifocal ground-glass opacities (GGOs) with patchy consolidations. Consequently, an increase in the number, size, and density of GGOs on chest CT was linked with disease development.[7] In addition, a number of studies have developed innovative techniques, such as an AI system using X-ray[8] and surface imaging technique,[9] which validate the medical evidence linking affected lungs for the early detection of COVID-19. Bio-detection applications are well-suited for nanomaterials and quantum dots. Wang et al. recently reported the facile fabrication technique for boron

Received: May 2, 2022
Accepted: June 10, 2022
Published: August 4, 2022

quantum dots.[10] Due to its outstanding photothermal properties, it may be employed for cancer cell identification and drug delivery. In addition, bioimaging and biosensing techniques enabled by metasurfaces have emerged as a viable way for disease detection. With the use of optical antennas, microelectromechanical systems, and sophisticated data processing, early disease detection is made considerably easier.[11]

Microstrip patch antennas are becoming immensely popular in biomedical applications due to their major characteristics, such as lower profile, agreeable to planar, non-planar exterior, simple and uncomplicated fabrication, and vigorous design. Many researchers have investigated the use of microstrip patch antennas for the early detection of breast cancer,[12,13] brain tumor,[14,15] lung cancer,[16] and many other biomedical applications.[17,18] Patch antennas are preferred over others for biomedical applications due to their low weight, thin profile, linear and circular polarization, dual and multi-frequency operation capacity, and ease of fabrication.[19−21] Different materials are frequently used in patch antenna design, such as copper,[22−24] gold,[25−27] and aluminum.[28,29] However, the use of these conventional materials usually provides narrow bandwidth.[30,31] In recent years, many research groups have explored nanomaterials such as graphene,[32] ZnO nanorods,[33] TiO_2,[34] multiwall carbon nanotubes (MWCNTs),[31,35] and so forth, designing the radiating element of the patch antenna. Besides, these nanomaterials have been used in many other photothermal[36−40] and optical device applications.[41−43] Among these, MWCNTs possess the potential to be used to design wide bandwidth patch antenna due to their superior alternating current conductivity and electromagnetic wave interactions. Since the discovery of the MWCNTs in 1991, they has demonstrated their superiority in the wide range of applications because of their superior electromechanical and optical properties. Herein, we utilize MWCNT material to form a radiating patch because its conductivity and electromagnetic wave interactions are better than conventional conductor copper. Carbon nanotubes (CNTs) are especially appealing at the nanoscale because of their outstanding mechanical, electrical, and thermal characteristics. The use of MWCNT-based antennas in low-power communication devices such as synthetic aperture radar in hostile chemical and gas environments is of special interest since traditional copper patches may oxidize in such conditions. Bandwidth improvement is a significant benefit of microstrip patch antennas for a higher data transmission rate. Since the diagnosis of COVID-19 disease is now a global challenge, we propose implementing an on-body patch antenna with high conductive MWCNT-based radiating patch capable of operating at ultrawide band (UWB) frequency on the COVID-19-affected lung phantom model. UWB uses high frequencies that can provide spatial and directional data and also much better at ranging with greater accuracy of data transmission, low power consumption, and good ability of penetration for human tissue. Besides, owing to its low power and non-ionizing property, it does not have any biological side effects on the human tissue.[44,45]

In this work, we report the application of a microstrip patch antenna with UWB frequency for detecting COVID-19-affected lungs. The antenna's radiating element (patch) consisted of MWCNTs, a highly conductive and flexible material embedded on the top layer of a lossy substrate. Radiating properties such as the return loss rate (S_{11}), the voltage standing wave ratio (VSWR), the far-field radiation pattern, and directivity of the antenna were characterized under free space, which agreed well with the simulation results. A lung phantom model with normal tissues and infected tissues was modeled in CST microwave studio software to analyze the antenna performance. Finally, the antenna was demonstrated on a normal lung and on a COVID-19-affected lung to maintain the same spectral properties. The value of the specific absorption rate (SAR) is also computed for the safety measurement on human body applications of the antenna. As the proposed antenna would be utilized to identify COVID-19-infected lungs at an early stage, it will aid in prioritizing patients' treatment and investigation depending on the severity of their lung condition. Therefore, the suggested technique will not replace the current method but will assist in the initial identification of COVID-19 patients and setting treatment priorities depending on lung condition. This advancement will allow it to be used in many resource-constrained places where conventional X-ray, CT scans, and other medical facilities to diagnose the COVID-19-affected lung are scarce. Because of the significantly lower cost of fabrication, satisfactory performance, and faster response, it may be employed as an initial screening device for COVID-19 patients. Since the suggested method yields rapid results, the deployment of the proposed system would minimize the hospital workload, patient waiting time, and expenses. It will also aid in effectively isolating and quarantining COVID-19-infected individuals, hence preventing the virus's widespread transmission.

EXPERIMENTAL SECTION

Materials. MWCNT powder was purchased from Six Carbon Inc., and the ethyl alcohol (80%), acetone, and isopropyl alcohol (IPA) were purchased from Sigma-Aldrich. The flame retardant 4 (FR4) substrate (3.26 mm thickness) and the connector were purchased from the local market. All the chemicals were used as received without further purification.

Antenna Fabrication. At first, an 80 mm^2 rectangular area was cut from the FR4 substrate. Then, the FR4 substrate was cleaned using acetone, followed by several ethyl alcohol treatments. After that, the substrate was washed several times using DI water and dried in an oven at 55 °C for 4 h. The MWCNT powder was mixed with IPA at a ratio of 1 mg mL^{-1}, and the solution was stirred ultrasonically for 4 h at 400 W output power and 40 kHz frequency. The as-prepared solution was used for the spin coating on the FR4 substrate. A few drops of MWCNT solution were dropped on the FR4 substrate using a pipette, and the FR4 substrate experienced 1500 rpm rotation for 30 s using a spin coater. The process was repeated several times until the deposition of the MWCNT was visible with bare eyes on the FR4 substrate. Finally, the MWCNT spin-coated on the FR4 substrate was dried in an oven at 55 °C for 2 h.

Material Characterizations. Transmission electron microscopy (TEM, JEOL model JEM-2010) was used to observe the TEM and high-resolution TEM (HRTEM) images of MWCNTs. The microstructures of the as-prepared MWCNT were observed by scanning electron microscopy (SEM; TESCAN, VEGA3) with an acceleration voltage of 20 kV. The Raman peak was obtained using a Raman spectroscope (WITEC confocal Raman system) equipped with a 532 nm laser source.

https://doi.org/10.1021/acsomega.2c02550
ACS Omega 2022, 7, 28265−28274

RESULTS AND DISCUSSION

The proposed microstrip patch antenna consists of a radiating patch made of a thin layer of 1.65 mm of the MWCNT, deposited on a uniform layer of the FR4 dielectric substrate by the spin-coating method. Copper was used as the ground of the antenna. The preparation process of the antenna is illustrated in Figure 1a. The SEM image shows the uniform

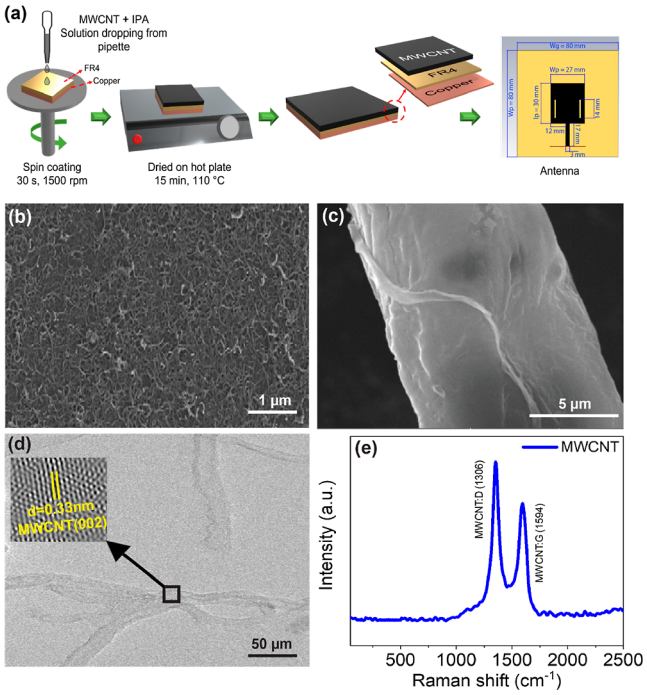

Figure 1. (a) Fabrication process of the proposed microstrip patch antenna; (b,c) SEM image of the MWCNT deposited on top of the FR4 substrate at different magnitudes; (d) TEM image of the MWCNT. HRTEM image is shown in the inset; and (e) Raman spectra of the MWCNT.

deposition of the MWCNT film on the FR4 substrate. Figure 1b,c depicts SEM images at different magnifications. The TEM and HRTEM images of randomly selected areas are shown in Figure 1d. The interplanar spacing of 0.33 nm is measured from the HRTEM image, which matches the (002) plane of the MWCNT. The Raman spectrum in Figure 1e shows that the peaks at 1306 and 1594 cm^{-1} correspond to the D and G band vibrational modes of the MWCNT. The high conductivity offered by the MWCNT helps lessen the return loss of the proposed antenna.[30,46] Unlike the conventional conductor-based antenna, the performance of the MWCNT-based patch antenna does not deteriorate or oxidize in gas or hard conditions.[30] The superior conductivity (4949 S/m) and higher thermal conductance (2586 W K^{-1} m^{-1}) help reduce return losses. The patch, substrate, and ground material parameters are presented in Table S1 (Supporting Information). The proposed MWCNT patch antenna is shown in Figure 2a,b, which operates at an UWB frequency of 6.63 GHz in free space and 7.29 GHz in normal lung phantom. The proposed microstrip-patch antenna with both the length and width of 80 mm was designed by using CST microwave studio software.

When the antenna is designed, the total thickness is maintained 3.31 mm (1.655 + 1.62 + 0.035 mm) and the dimension is 80 × 80 × 3.31 mm (21,184 mm^3) to reduce the

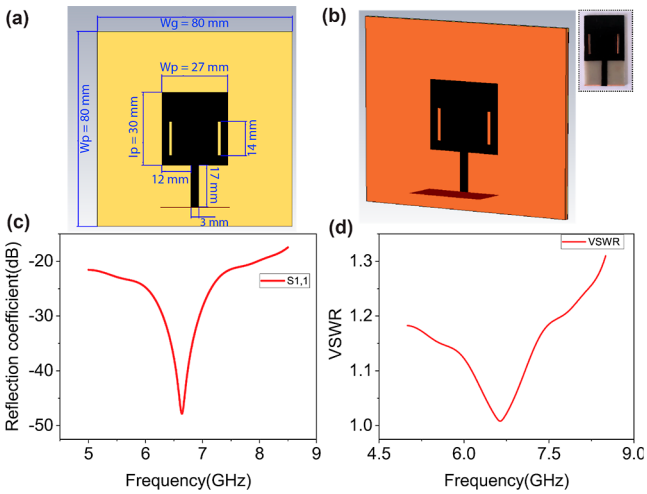

Figure 2. (a) Antenna measurement diagram; (b) MWCNT antenna simulated in CST microwave studio software (inset: practically implemented MWCNT antenna); (c) S_{11} (return loss) is −47.92 dB at 6.63 GHz in free space; and (d) VSWR is 1.008 at 6.63 GHz in free space.

effects of a high conductive human tissue as well as to avoid shortening the antenna. A lung phantom model with normal and pneumonia (COVID-19)-affected tissues is created along with the designed antenna. We check its biocompatibility property by locating the antenna in the distinct model where the values are kept in the millimeter range, designing the antenna. Using eqs S1−S4 (Supporting Information), the width and length of the patch antenna were determined as 27 and 30 mm, respectively. The various dimensions of the antenna are shown in Figure 2a. The waveguide port positioning at the antenna with a feed line placed in the central part of the antenna is shown in Figure 2b. The waveguide port is linked with input power, the downward of the feed line, where the width and length of the microstrip feedline are 3.18 and 17.1 mm, respectively. The waveguide port is indicated by the red segment in Figure 2b, and the input impedance of the feedline or inset fed is considered as 50 Ω.

The designed antenna was first put to the test in an indoor environment. After that, a normal lung phantom model is produced. Following that, the designed antenna was attached to a normal lung phantom. Later, a lung phantom with the affected condition is developed, and the designed antenna is put and tested on it. In free space, the operating frequency of our designed antenna is 6.63 GHz. In this frequency, the value of return loss or S_{11} parameter is measured −47.92 dB, which is shown in Figure 2c. Return loss shows how much power is reflected because of the discontinuity of impedance. If an antenna has a return loss above −10 dB, it is not acceptable for transmission. Hence, the standard limit for return loss is −10 dB,[47] which indicates that our designed antenna has less return loss and will perform well in free space. VSWR determines the impedance match of antenna with the transmission line where it is connected. Usually, if the VSWR value is under 2, it is regarded as a better antenna.[48] The highest value of VSWR in free space was determined as 1.004, as shown in Figure 2d.

Figure 3a,b provides the far-field radiation and gain values. Gain is one of the important parameters to measure the antenna performance, and it is related to directivity.[49,50] The gain for the antenna in free space is 8.865 dB, which is quite

https://doi.org/10.1021/acsomega.2c02550
ACS Omega 2022, 7, 28265−28274

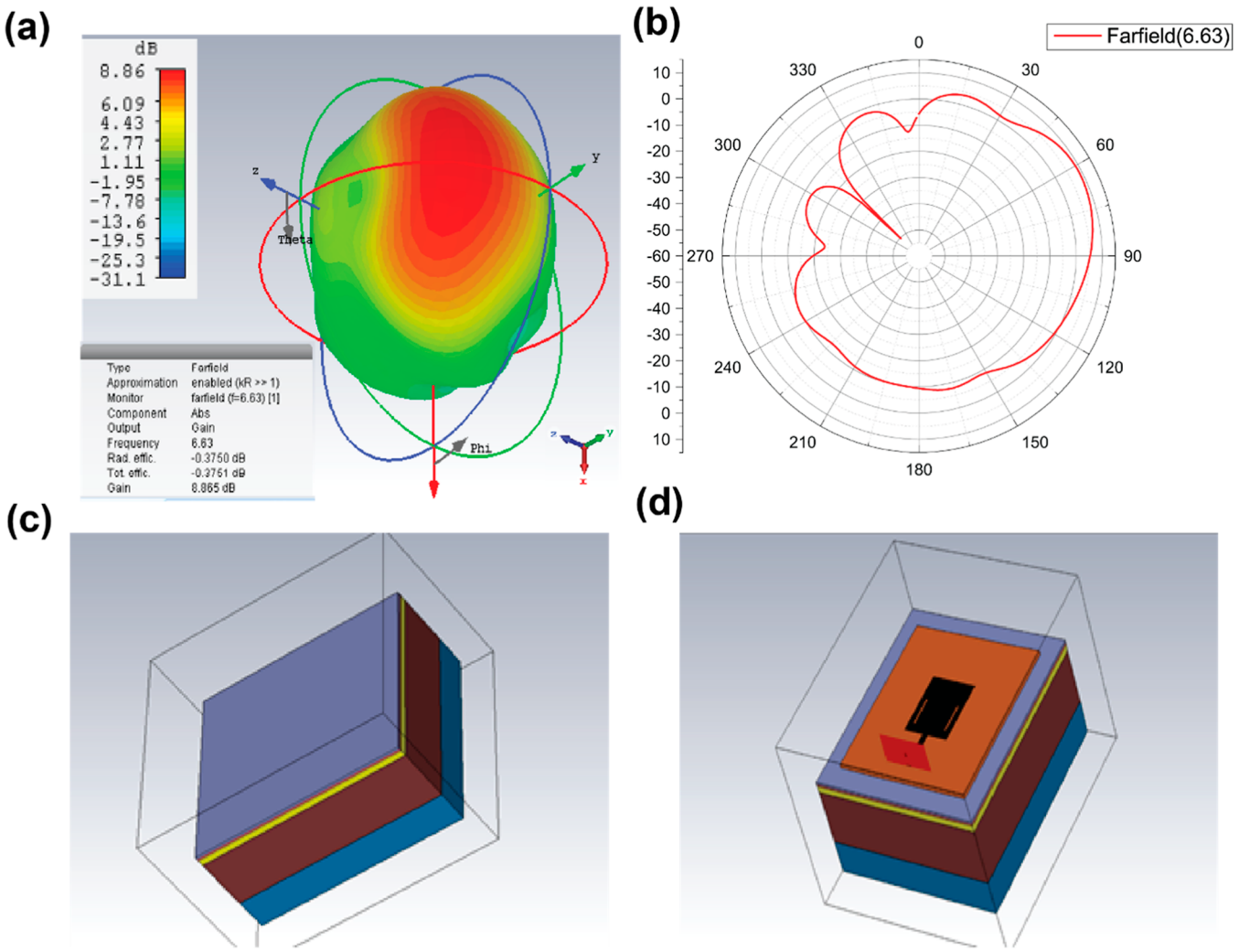

Figure 3. (a) Radiation pattern (3D) in free space; (b) radiation pattern (2D) in free space; (c) designed normal lung phantom model; and (d) antenna placed on normal lung tissue.

Table 1. Normal Lung Properties of Different Tissue Layers

	permeability (ε)	electric conductivity (S/m)	density (kg/m^3)	thermal conductance (W/K/m)	heat capacity (kJ/K/kg)	diffusivity (m^2/s)	blood flow (W/K/m^3)	metabolic rate (W/m^3)	size (mm)
skin	34.946	3.8912	1100	0.50	3.5	7.6×10^{-8}	9100	1620	1
fat	4.9367	0.30623	910	0.24	2.5	8.8×10^{-8}	1700	300	3
muscle	48.217	5.2019	1041	0.56	3.7	1.4×10^{-7}	2700	480	25
lung	18.394	2.1695	1020	0.48	3.8	1.7×10^{-7}	9500	1700	15

good, and the directivity is 9.240 dBi. Therefore, the antenna efficiency is found 95.94% for free space.

The respiratory system can be affected in various ways by COVID-19 according to the immunity system of the person, age, and so forth. Specially, it gets worse for those who have already been suffering from lung disease. It can cause chronic obstructive pulmonary disease, asthma, and interstitial lung disease problems.[51] To analyze the biocompatibility of mentioned antenna, a normal lung of the human phantom model is created in CST software, as shown in Figure 3c. Next, the designed antenna has been placed on the lung model to observe the antenna performance, as shown in Figure 3d. There are several layers of tissues in the human body and a set of parameters for those related tissues. Each of them has unique properties, and values differ from one another. Following Table 1 shows all the necessary tissue layers and their properties for creating a normal lung phantom.

After placing the antenna in a normal lung phantom, the antenna's operating frequency has shifted to 7.29 GHz, which is within the limit of UWB frequency. The necessary antenna

Table 2. Performance Analysis of Different Tissue Layers

parameters	free space	normal lung	COVID-19-affected lung (2 mm fluid)	COVID-19-affected lung (5 mm fluid)
S_{11}	−47.92 dB	−48.52 dB	−40.12 dB	−39.95 dB
operating frequency	6.63 GHz	7.29 GHz	7.29 GHz	7.22 GHz
VSWR	1.008	1.007	1.04	1.02

https://doi.org/10.1021/acsomega.2c02550
ACS Omega 2022, 7, 28265−28274

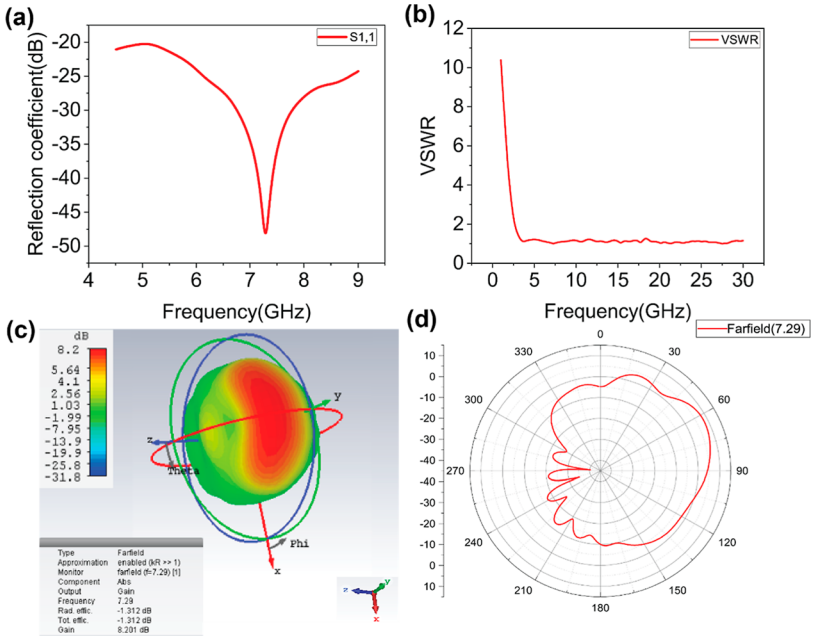

Figure 4. (a) S_{11} (return loss) is −48.52 dB at 7.29 GHz in normal lung phantom; (b) VSWR is 1.007 at 7.29 GHz on normal lung; (c) radiation pattern (3D) on normal lung; and (d) radiation pattern (2D) on normal lung.

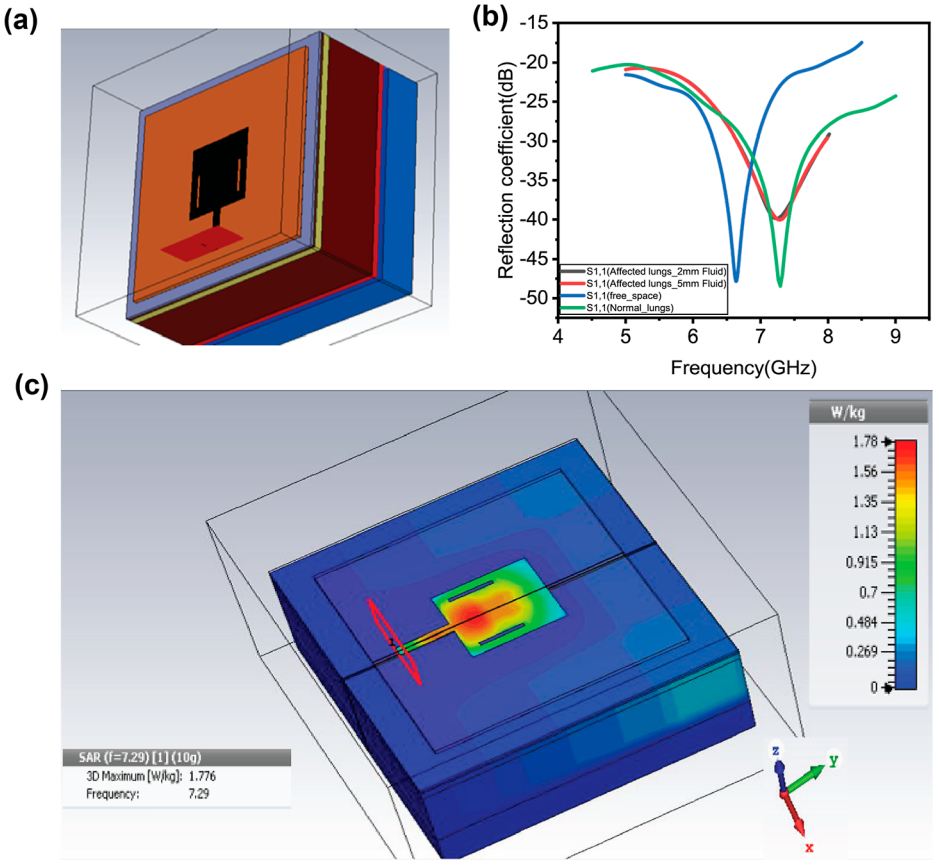

Figure 5. (a) Designed COVID-19-affected lung phantom by injecting the fluid layer and antenna placed on affected lung tissue; (b) S_{11} (return loss) of COVID-19-affected lungs with 2 and 5 mm fluid layers, S_{11} (return loss) of normal lung and in free space; and (c) SAR on the normal lung phantom model.

parameters are tested again. Such as, S_{11} or return loss in normal lung phantom is now measured −48.52 dB, as shown in Figure 4a. A higher return loss indicates better impedance matching. Previously, it was −47.92 dB in free space. On the other hand, the value of VSWR is observed 1.007, as shown in Figure 4b, which is desired. The gain found in normal lung is 8.201 dB, and the directivity is 9.513 dB, as shown in Figure 4c,d, representing the better antenna performance. Here, the

https://doi.org/10.1021/acsomega.2c02550
ACS Omega 2022, 7, 28265−28274

Table 3. Comparative Study of Antenna over Different Patch Materials

antenna type	size (mm)	application	material of patch (conductive material) (S/m)	operating frequency (GHz)	S_{11} (dB)	refs
rectangular patch antenna	30 × 30	MWCNT-based patch antenna for bandwidth enhancement	MWCNT	10	−11.64	30
rectangular patch antenna	33.6 × 41.7	design and development of $Ni_{0.75}Zn_{0.25}Fe_2O_4$/MWCNT microstrip patch antenna (MPA) for ISM band spectrum applications	$Ni_{0.75}Zn_{0.25}Fe_2O_4$/MWCNT	2.43	−24.03	31
rectangular patch antenna	30 × 30	MWCNT-based RF antennas	MWCNT	2.32	−19.5	57
square spiral trace truncated horizontally shaped patch antenna	80 × 80	a dual-frequency wearable MWCNT ink-based spiral microstrip antenna	MWCNT	2.47	−27	58
linear array antenna		early detection and monitoring of pulmonary oedema (lungs filled by water)	copper tape	0.096	−22.4	59
rectangular patch antenna	35 × 35 × 1.52	lung cancer detection	cooper	2.27	−19.35	60
rectangular patch antenna	32.7 × 44 × 5.0	telemedicine and mobile biomedical imaging systems	copper tape	6.301	−15.01	61
rectangular patch antenna	32.7 × 44 × 5.0	telemedicine and mobile biomedical imaging systems	graphene	5.28/8.225	−26.52/−29.88	61
rectangular patch antenna	32.7 × 44 × 5.0	telemedicine and mobile biomedical imaging systems	conductive bare	6.495	−24.89	61
cupcake shaped antenna	30 × 40 × 1.52	detection of lung cancer using the UVB	cooper	8.00	−15.73	62
rectangular patch antenna	36 × 60 × 1.6	detecting lung tumor	copper	5.02	−22.5	63
antenna array based on GCL	10 × 9 × 1.26	5G antenna application	graphene	26.0	−39.19 (in free space)	64
rectangular microstrip patch antenna	60 × 60 × 2	application as a frequency reconfigurable patch antenna for wearable electronics	silver ink polysiloxane	2.48	−23.5	65
rectangular strip patch antenna	80 × 80 × 3.31	COVID-19-affected lung detection using UWB frequency	SWCNT	1.31/1.29/6.28	−31.12/−32.44/−28.14	Supporting Information, Note S6
MWCNT rectangular strip patch antenna	**80 × 80 × 3.31**	**COVID-19-affected lung detection using UWB frequency**	**MWCNT**	**7.291/7.29/7.22**	**−48.52/−40.12/−39.95**	**this work**

https://doi.org/10.1021/acsomega.2c02550
ACS Omega 2022, 7, 28265−28274

efficiency of antenna has decreased to 86.30% after placing on a normal lung phantom.

The antenna was then put through once again by creating a COVID-19-affected phantom lung model by placing a fluid layer on top of the previously designed phantom lung with two different thicknesses of water and blood cells, as illustrated in Figure 5a. As previously stated, in the event of COVID-19, the respiratory system can be attacked by a cause of pneumonia, in which the lung becomes filled with a certain form of fluid or pus.[52,53] It is believed that they should be filled with fluid rather than water, which causes inflammation and shortness of breath. While making the affected lung phantom, a thick layer of blood and water was created for the purpose of making that particular fluid density of affected lung. In order to test the design, it was put on two distinct affected lung phantoms with varied fluid arrangement parameters. The fluids of phantom are 2 and 5 mm in size, respectively. As of now, there has not been a straightforward estimate for COVID-19-associated lung infection, which is why we decided to use two different fluid layer thicknesses for this experiment. Table S3 (Supporting Information) represents the parameters of the affected lung phantom.

After placing the antenna in these two affected lung models, it has been observed that our designed antenna provides a better S_{11} value of −40.12 and −39.95 dB at the frequencies of 7.29 and 7.22 GHz, respectively, which is shown in Figure 5b, and indicates that the designed antenna is working fine on the affected lung and which can be used for assisting in detecting the COVID-19 case.

Table 2 shows the summary of our MWCNT-based antenna performance in different environments. It has been clearly seen that the antenna initially operates in free space at 6.63 GHz frequency with an acceptable return loss of −47.92 dB, and after placing the antenna on a normal lung and affected phantom lung model, the frequency is shifted up to 7.29 GHz with the variation of suitable S_{11} values that ensures the biocompatibility of our designed antenna. Therefore, from this data table, we can appraise that the MWCNT material-based antenna is capable to diagnosis the affected lung caused by COVID-19.

SAR can be defined as when human tissue gets absorbed by the energy that is exposed in the electromagnetic field. International Commission on Non-Ionizing Radiation Protection (ICNIRP) determined the range for SAR to defend against harmful radiation to the human body. For 1 g of human tissue, the acceptable maximum SAR value is 1.6 W/kg, according to Federal Communications Commission (FCC), and for 10 g of human tissue, the maximum limit of SAR is 2.0 W/kg, in accordance to ICNIRP.[54] Therefore, SAR value analysis is important when any devices are put on human body tissue. As shown in Figure 5c, we obtained a SAR value of 1.77 W/kg for 10 g of tissue using only 1 mW of power during the experiments, which is suitable for the human body and satisfies the Federal Communications Commission (FCC) and IEEE standard for higher safety for medical applications for the human body and makes it biocompatible and safe.[47,55,56] This ensures that the proposed antenna is biocompatible and safe on the human body lungs. To compare the performance of the proposed MWCNT-based patch antenna for detecting COVID-19-affected lungs, a similar design was made using single-wall carbon nanotubes (SWCNTs), which is provided in Supporting Information Note S6. From the simulated data (Figures S2−S5, Supporting Information), it can be seen that the MWCNT-based patch antenna demonstrated better performance compared with SWCNTs. MWCNTs have a larger number of nanotubes on their surface for the same quantity of material as SWCNTs. As each nanotube on the surface resonates electromagnetic waves separately and influences the improvement of the bandwidth, a higher number of nanotubes offered by the MWCNT enables a wider bandwidth than that of the SWCNT-based radiating patch antenna. Furthermore, Table 3 presents a comparative analysis of patch antennas made from various materials, primarily for biomedical applications, with the proposed rectangular patch antenna made with MWCNTs having a wider operating frequency than others. The significantly increased bandwidth of the proposed antenna owing to the use of MWCNT in the radiating patch, usage of UWB frequency, and decreased return loss (S_{11} parameter) all contribute to achieving superior performances.

CONCLUSIONS

The performance of the MWCNT-based patch antenna for detecting COVID-19-affected lungs has been demonstrated here. Various parameters of the designed antenna such as resonant frequency, return loss, and VSWR are observed to be 7.29 GHz, −40.12 dB, and 1.04, respectively, placed on the phantom model, indicating the better performance of the designed antenna. SAR is also calculated at 7.29 GHz to ensure that the safety is obtained at 1.77 W/kg for 10 g of tissues. The MWCNT-based patch antenna is also successfully fabricated using a cost-effective spin-coating method, which can be employed for mass production. The proposed antenna exhibits superior performance over the UWB frequency of 6.63−7.29 GHz, demonstrating the potential applicability for other medical applications. After all of these parameter value analyses and comparisons are completed, it is anticipated that the proposed antenna may be utilized as an on-body antenna for the initial detection of COVID-19-affected lungs.

ASSOCIATED CONTENT

Supporting Information

The Supporting Information is available free of charge at https://pubs.acs.org/doi/10.1021/acsomega.2c02550.

Material properties; properties of materials used for the antenna design; equations for calculating antenna parameters; antenna design measurements; geometrical measurement value of antenna; fluid properties; properties of fluid for the COVID-19-affected lung phantom model; MWCNT antenna placed on COVID-19-affected lung phantom when the volume of infection (fluid) is half of the lung return loss obtained −32.72 dB at 6.29 GHz frequency in COVID-19-affected lung phantom when the volume of infection (fluid) is half of the lung material properties (SWCNTs); properties of SWCNT materials used for patch design; SWCNT-based antenna design and analysis; SWCNT-based patch antenna; return loss obtained −31.122 dB in free space at 1.32 GHz frequency; VSWR obtained 1.057 in free space at 1.32 GHz frequency; return loss obtained −32.122 dB in the lung phantom model at 1.29 GHz frequency; VSWR obtained 1.048 in the lung phantom model at 1.29 GHz frequency; SWCNT-based antenna placed on COVID-19-affected lung phantom; return loss obtained −28.14 dB at 6.28 GHz frequency in the

https://doi.org/10.1021/acsomega.2c02550
ACS Omega 2022, 7, 28265−28274

COVID-19-affected lung phantom model by placing SWCNT antenna; results; and comparative analysis of MWCNT-based patch antenna to SWCNT-based patch antenna (PDF)

AUTHOR INFORMATION

Corresponding Author

Yuen Hong Tsang − *Department of Applied Physics and Materials Research Center, The Hong Kong Polytechnic University, Kowloon 999077, Hong Kong; Shenzhen Research Institute, The Hong Kong Polytechnic University, Shenzhen 518057, People's Republic of China;* orcid.org/0000-0001-5632-5224; Email: yuen.tsang@polyu.edu.hk

Authors

Raja Rashidul Hasan − *Department of Electrical and Electronic Engineering, American International University-Bangladesh (AIUB), Dhaka 1229, Bangladesh*

Ahmed Mortuza Saleque − *Department of Applied Physics and Materials Research Center, The Hong Kong Polytechnic University, Kowloon 999077, Hong Kong; Shenzhen Research Institute, The Hong Kong Polytechnic University, Shenzhen 518057, People's Republic of China;* orcid.org/0000-0002-2124-8721

Afrin Binte Anwar − *Department of Electrical and Electronic Engineering, American International University-Bangladesh (AIUB), Dhaka 1229, Bangladesh*

Md. Abdur Rahman − *Department of Electrical and Electronic Engineering, American International University-Bangladesh (AIUB), Dhaka 1229, Bangladesh*

Complete contact information is available at: https://pubs.acs.org/10.1021/acsomega.2c02550

Author Contributions

‖R.R.H. and A.M.S. equally contributed to this work.

Notes

The authors declare no competing financial interest.

ACKNOWLEDGMENTS

This work is financially supported by the Research Grants Council of Hong Kong, China (project number: 152093/18E), the Hong Kong Polytechnic University (project number: 1-ZE14), and the Hong Kong Polytechnic University Shenzhen Research Institute, Shenzhen, China [grant code: The Science and Technology Innovation Commission of Shenzhen (JCY20180306173805740)].

REFERENCES

(1) Elezkurtaj, S.; Greuel, S.; Ihlow, J.; Michaelis, E. G.; Bischoff, P.; Kunze, C. A.; Sinn, B. V.; Gerhold, M.; Hauptmann, K.; Ingold-Heppner, B.; Miller, F.; Herbst, H.; Corman, V. M.; Martin, H.; Radbruch, H.; Heppner, F. L.; Horst, D. Causes of Death and Comorbidities in Hospitalized Patients with COVID-19. *Sci. Rep.* **2021**, *11*, 4263.

(2) Armstrong, D. The COVID-19 Pandemic and Cause of Death. *Sociol. Health Illn.* **2021**, *43*, 1614−1626.

(3) Sun, Q.; Qiu, H.; Huang, M.; Yang, Y. Lower Mortality of COVID-19 by Early Recognition and Intervention: Experience from Jiangsu Province. *Ann. Intensive Care* **2020**, *10*, 33.

(4) Vianello, C.; Strozzi, F.; Mocellin, P.; Cimetta, E.; Fabiano, B.; Manenti, F.; Pozzi, R.; Maschio, G. A Perspective on Early Detection Systems Models for COVID-19 Spreading. *Biochem. Biophys. Res. Commun.* **2021**, *538*, 244−252.

(5) Rahman, T.; Khandakar, A.; Qiblawey, Y.; Tahir, A.; Kiranyaz, S.; Abul Kashem, S. B.; Islam, M. T.; Al Maadeed, S.; Zughaier, S. M.; Khan, M. S.; Chowdhury, M. E. H. Exploring the Effect of Image Enhancement Techniques on COVID-19 Detection Using Chest X-Ray Images. *Comput. Biol. Med.* **2021**, *132*, 104319.

(6) Xu, G.; Yang, Y.; Du, Y.; Peng, F.; Hu, P.; Wang, R.; Yin, M.; Li, T.; Tu, L.; Sun, J.; Jiang, T.; Chang, C. Clinical Pathway for Early Diagnosis of COVID-19: Updates from Experience to Evidence-Based Practice. *Clin. Rev. Allergy Immunol.* **2020**, *59*, 89−100.

(7) Zu, Z. Y.; Jiang, M. D.; Xu, P. P.; Chen, W.; Ni, Q. Q.; Lu, G. M.; Zhang, L. J. Coronavirus Disease 2019 (COVID-19): A Perspective from China. *Radiology* **2020**, *296*, E15−E25.

(8) Mishra, M.; Parashar, V.; Shimpi, R. Development and Evaluation of an AI System for Early Detection of Covid-19 Pneumonia Using X-Ray (Student Consortium). In *2020 IEEE Sixth International Conference on Multimedia Big Data (BigMM)*; IEEE, 2020; pp 292−296.

(9) Poggiali, E.; Dacrema, A.; Bastoni, D.; Tinelli, V.; Demichele, E.; Mateo Ramos, P.; Marcianò, T.; Silva, M.; Vercelli, A.; Magnacavallo, A. Can Lung US Help Critical Care Clinicians in the Early Diagnosis of Novel Coronavirus (COVID-19) Pneumonia? *Radiology* **2020**, *295*, No. E6.

(10) Wang, C.; Chen, Q.; Chen, Q.; Chen, H.; Liu, J.; Song, Y.; Liu, J.; Li, D.; Ge, Y.; Gong, Y.; Zhang, Y.; Zhang, H. Boron Quantum Dots All-Optical Modulator Based on Efficient Photothermal Effect. *Opto-Electron. Adv.* **2021**, *4*, 200032.

(11) Chen, L.; Li, Y.; Hong, M. Total Reflection Metasurface with Pure Modulated Signal. *Adv. Opt. Mater.* **2019**, *7*, 1801130.

(12) Aziz, A.; Ahmad, D.; Shila, T. A.; Rana, S.; Hasan, R. R.; Rahman, M. A. On-Body Circular Patch Antenna for Breast Cancer Detection. In *2019 IEEE International Electromagnetics and Antenna Conference (IEMANTENNA)*; IEEE, 2019; pp 029−034.

(13) Padmavathy, T. V.; Venkatesh, P.; Bhargava, D.; Sivakumar, N. Design of I-Shaped Dual C-Slotted Rectangular Microstrip Patch Antenna (I-DCSRMPA) for Breast Cancer Tumor Detection. *Clust. Comput.* **2019**, *22*, 13985−13993.

(14) Sinha, S.; Niloy, T.-S. R.; Hasan, R. R.; Rahman, M. A.; Rahman, S. A Wearable Microstrip Patch Antenna for Detecting Brain Tumor. In *2020 International Conference on Computation, Automation and Knowledge Management (ICCAKM)*; IEEE, 2020; pp 85−89.

(15) Elkorany, A. S.; Helmy, R. M.; Saleeb, A. A.; Areed, N. F. Microstrip Patch Antenna Linear Arrays for Brain Tumor Detection. In *2019 14th International Conference on Computer Engineering and Systems (ICCES)*; IEEE, 2019; pp 425−431.

(16) Bait-Suwailam, M. M.; Al-Busaidi, O.; Al-Shahimi, A. A Low-Cost Microwave Sensing Platform for Water Accumulation Abnormality Detection in Lungs. *Microw. Opt. Technol. Lett.* **2018**, *60*, 1295−1300.

(17) Yang, Z.-J.; Xiao, S.-Q.; Zhu, L.; Wang, B.-Z.; Tu, H.-L. A Circularly Polarized Implantable Antenna for 2.4-GHz ISM Band Biomedical Applications. *IEEE Antennas Wirel. Propag. Lett.* **2017**, *16*, 2554−2557.

(18) Markkandan, S.; Malarvizhi, C.; Raja, L.; Kalloor, J.; Karthi, J.; Atla, R. Highly Compact Sized Circular Microstrip Patch Antenna with Partial Ground for Biomedical Applications. *Mater. Today: Proc.* **2021**, *47*, 318−320.

(19) Wang, B.; Lin, X. Q.; Yang, X. Dual-Band Wide-Angle Scanning Phased Array Composed of Stacked Patch Antennas. In *2020 International Conference on Microwave and Millimeter Wave Technology (ICMMT)*; IEEE, 2020; pp 1−3.

(20) Liu, N.-W.; Zhu, L. Single-Layer Low-Profile Patch Antennas with Improved CP Performance by Using Multiresonant Modes (Invited Paper). In *2020 IEEE Asia-Pacific Microwave Conference (APMC)*; IEEE, 2020; pp 231−233.

(21) Parasuraman, S.; Yogeeswaran, S.; Ramesh, G. P. Design of Microstrip Patch Antenna with Improved Characteristics and Its Performance at 5.1GHz for Wireless Applications. *IOP Conf. Ser.: Mater. Sci. Eng.* **2020**, *925*, 012005.

(22) Atser, A. R.; Mom, J. M.; Igwue, G. A. The Comparative Analysis of Graphene Nano-Based and Copper Nano-Based Patched Antenna Using HFSS. *IOP Conf. Ser. Earth Environ. Sci.* **2021**, *730*, 012020.
(23) Suresh babu, T. N.; Sivakumar, D. Stepped Slot Patch Antenna with Copper Ground Plane and Solar Cell Ground Plane for Future Mobile Communications. *Prog. Electromagn. Res. C* **2020**, *98*, 187−198.
(24) Miranda, I. R. S.; Sousa, F. M. d.; de Sousa, F. B.; Oliveira, J. E. d.; Costa, M. B. C. Microstrip Patch Antenna with BiNbO4(V2O5) Substrate and Copper Periodic Structures. *Mater. Res.* **2021**, *24*, No. e20200487.
(25) Ambalg, A. P.; Sujata, S. K. Analysis of 8.71 GHz Operated Gold Nanoparticles Based Multi-Slotted Patch Antenna Etched on Epoxy Dielectric Material Having Broadsided Radiation Characteristics. *Mater. Today: Proc.* **2021**, *43*, 3810−3814.
(26) Abohmra, A.; Abbas, H.; Kazim, J. u. R.; Rabbani, M. S.; Li, C.; Alomainy, A.; Imran, M. A.; Abbasi, Q. H. An Ultrawideband Microfabricated Gold-Based Antenna Array for Terahertz Communication. *IEEE Antennas Wirel. Propag. Lett.* **2021**, *20*, 2156.
(27) Salehi, M.; Abbasian, K.; Pourziad, A. 2D-Photonic Crystal Based Bowtie Nano Antenna Designing with Spherical Gold Particles for Terahertz Applications. In *2020 28th Iranian Conference on Electrical Engineering (ICEE)*; IEEE, 2020; pp 1−4.
(28) Siragam, S.; Dubey, R. S.; Pappula, L. Analysis of Dielectric Properties of Zinc Aluminum Silicate Based Ceramic Nanoparticles. *Mater. Today: Proc.* **2021**, *45*, 2801−2808.
(29) Choi, J.; Choi, J.; Hwang, W. Miniature Millimeter-Wave 5G Antenna Fabricated Using Anodized Aluminum Oxide for Mobile Devices. *ACS Omega* **2020**, *5*, 26206−26210.
(30) Chaya Devi, K. S.; Angadi, B.; Mahesh, H. M. Multiwalled Carbon Nanotube-Based Patch Antenna for Bandwidth Enhancement. *Mater. Sci. Eng., B* **2017**, *224*, 56−60.
(31) Syazwan, M. M.; Hapishah, A. N.; Hamidon, M. N.; Ismail, I.; Hasan, I. H. Design and Development of Ni0.75Zn0.25Fe2O4/MWCNT Microstrip Patch Antenna (MPA) for ISM Band Spectrum Applications. *Synth. Met.* **2021**, *271*, 116630.
(32) Singla, A.; Marwaha, A.; Marwaha, S. Graphene as a Shielding Material for SAR Reduction in Human Head Using Rectangular and Circular Patch Antenna. *Karbala Int. J. Mod. Sci.* **2021**, *7*, 169−175.
(33) Kashyap, P. A.; Das, S. R.; Baruah, S. *Nanomaterial-Based Microstrip Patch Antenna Array for X Band Operation*; Springer, 2021; pp 65−76.
(34) Ambalgi, A. P.; Kamalapurkar, S. S.; Hunagund, P. V.; Patil, R. Design, Modeling and Experimental Study of GHz Patch Antenna Coated with Conductive Layer of Nanomaterial for Enhanced Characteristics with Defected Ground Structure in Communication Network Applications. *SN Comput. Sci.* **2021**, *2*, 152.
(35) Suryanarayana, V.; Satya Anuradha, M.; Douglas, S. P. Bandwidth Enhancement of Multiwalled Carbon Nanotube Antenna Using Structural Modifications and DGS in X-Band Applications. In *2021 International Conference on Computing, Communication, and Intelligent Systems (ICCCIS)*; IEEE, 2021; pp 792−797.
(36) Saleque, A. M.; Ahmed, S.; Ivan, M. N. A. S.; Hossain, M. I.; Qarony, W.; Cheng, P. K.; Qiao, J.; Guo, Z. L.; Zeng, L.; Tsang, Y. H. High-Temperature Solar Steam Generation by MWCNT-HfTe2 van Der Waals Heterostructure for Low-Cost Sterilization. *Nano Energy* **2022**, *94*, 106916.
(37) Saleque, A. M.; Ahmed, S.; Ivan, M. N. A. S.; Hossain, M. I.; Qarony, W.; Tsang, Y. H. Localized Surface Plasmon Resonance Induced Temperature Enhancement by MWCNT-HfTe2 van Der Waals Heterostructure. In *2D Photonic Materials and Devices V*; Majumdar, A., Torres, C. M., Deng, H., Eds.; SPIE, 2022; p 39.
(38) Saleque, A. M.; Ma, S.; Ahmed, S.; Hossain, M. I.; Qarony, W.; Tsang, Y. H. Solar Driven Interfacial Steam Generation Derived from Biodegradable Luffa Sponge. *Adv. Sustainable Syst.* **2021**, *5*, 2000291.
(39) Saleque, A. M.; Nowshin, N.; Ivan, M. N. A. S.; Ahmed, S.; Tsang, Y. H. Natural Porous Materials for Interfacial Solar Steam Generation toward Clean Water Production. *Sol. RRL* **2022**, *6*, 2100986.
(40) Ivan, M. N. A. S.; Saleque, A. M.; Ahmed, S.; Cheng, P. K.; Qiao, J.; Alam, T. I.; Tsang, Y. H. Waste Egg Tray and Toner-Derived Highly Efficient 3D Solar Evaporator for Freshwater Generation. *ACS Appl. Mater. Interfaces* **2022**, *14*, 7936−7948.
(41) Ahmed, S.; Qiao, J.; Cheng, P. K.; Saleque, A. M.; Ivan, M. N. A. S.; Alam, T. I.; Tsang, Y. H. Two-Dimensional Gallium Sulfide as a Novel Saturable Absorber for Broadband Ultrafast Photonics Applications. *ACS Appl. Mater. Interfaces* **2021**, *13*, 61518−61527.
(42) Cheng, P. K.; Ahmed, S.; Qiao, J.; Wong, L. W.; Yuen, C. F.; Saleque, A. M.; Ivan, M. N. A. S.; Hani, S. U.; Hossain, M. I.; Zhao, J.; Wen, Q.; Tsang, Y. H. Nonlinear Optical Properties of Two-Dimensional Palladium Ditelluride (PdTe2) and Its Application as Aerosol Jet Printed Saturable Absorbers for Broadband Ultrafast Photonics. *Appl. Mater. Today* **2022**, *26*, 101296.
(43) Ahmed, S. M. M.; Al-Amin, M. R.; Ahammed, S.; Ahmed, F.; Saleque, A. M.; Abdur Rahman, M. Design, Construction and Testing of Parabolic Solar Cooker for Rural Households and Refugee Camp. *Sol. Energy* **2020**, *205*, 230−240.
(44) D'Amico, S.; De Matteis, M.; Rousseaux, O.; Philips, K.; Gyselinck, B.; Neirynck, D.; Baschirotto, A. Ultra Wide Band in Medical Applications. In *Advances in Biomedical Sensing, Measurements, Instrumentation and Systems*; Mukhopadhyay, S. C., Lay-Ekuakille, A., Eds.; Springer Berlin Heidelberg: Berlin, Heidelberg, 2010; pp 43−60.
(45) Alghanimi, A. H. Medical Application of Ultra-Wideband Technology. In *Innovations in Ultra-Wideband Technologies*; IntechOpen, 2021.
(46) Zahir, H.; Wojkiewicz, J. L.; Alexander, P.; Kone, L.; Belkacem, B.; Bergheul, S.; Lasri, T. Design Fabrication and Characterisation of Polyaniline and Multiwall Carbon Nanotubes Composites-based Patch Antenna. *IET Microw. Antennas Propag.* **2016**, *10*, 88−93.
(47) Sinha, S.; Hasan, R. R.; Niloy, T.-S. R.; Rahman, M. A. Antenna Design and Fabrication for Biotelemetry Applications. *Int. J. Electr. Comput. Eng.* **2021**, *11*, 3639.
(48) Sinha, S.; Hasan, R. R.; Niloy, T.-S. R.; Rahman, M. A. Antenna Design and Fabrication for Biotelemetry Applications. *Int. J. Electr. Comput. Eng.* **2021**, *11*, 3639.
(49) Modi, A. Y.; Alyahya, M. A.; Balanis, C. A.; Birtcher, C. R. Metasurface-Based Method for Broadband RCS Reduction of Dihedral Corner Reflectors With Multiple Bounces. *IEEE Trans. Antennas Propag.* **2020**, *68*, 1436−1447.
(50) Castorina, G.; Di Donato, L.; Morabito, A. F.; Isernia, T.; Sorbello, G. Analysis and Design of a Concrete Embedded Antenna for Wireless Monitoring Applications [Antenna Applications Corner]. *IEEE Antennas Propag. Mag.* **2016**, *58*, 76−93.
(51) Gong, J.; Dong, H.; Xia, Q.; Huang, Z.; Wang, D.; Zhao, Y.; Liu, W.; Tu, S.; Zhang, M.; Wang, Q.; Lu, F. Correlation analysis between disease severity and inflammation-related parameters in patients with COVID-19: a retrospective study. *BMC Infect. Dis.* **2020**, *20*, 963.
(52) Mizgerd, J. P. Inflammation and Pneumonia. *Clin. Chest Med.* **2018**, *39*, 669−676.
(53) Aquino-Martinez, R.; Hernández-Vigueras, S. Severe COVID-19 Lung Infection in Older People and Periodontitis. *J. Clin. Med.* **2021**, *10*, 279.
(54) Iqbal-Faruque, M. R.; Aisyah-Husni, N.; Ikbal-Hossain, M.; Tariqul-Islam, M.; Misran, N. Effects of Mobile Phone Radiation onto Human Head with Variation of Holding Cheek and Tilt Positions. *J. Appl. Res. Technol.* **2014**, *12*, 871−876.
(55) Bailey, W. H.; Harrington, T.; Hirata, A.; Kavet, R. R.; Keshvari, J.; Klauenberg, B. J.; Legros, A.; Maxson, D. P.; Osepchuk, J. M.; Reilly, J. P.; Tell, R. R. A.; Bodemann, R.; Thansandote, A.; Yamazaki, K.; Ziskin, M. C.; Zollman, P. M.; Bushberg, J.; Chou, C.-K.; Cleveland, R.; Faraone, A.; Foster, K. R.; Gettman, K. E.; Graf, K. Synopsis of IEEE Std C95.1-2019 "IEEE Standard for Safety Levels with Respect to Human Exposure to Electric, Magnetic, and

https://doi.org/10.1021/acsomega.2c02550
ACS Omega 2022, 7, 28265−28274

Electromagnetic Fields, 0 Hz to 300 GHz". *IEEE Access* **2019**, *7*, 171346−171356.
(56) Bernhardt, J. H. The New ICNIRP Guidelines: Criteria, Restrictions, and Dosimetric Needs. In *Radio Frequency Radiation Dosimetry and Its Relationship to the Biological Effects of Electromagnetic Fields*; Springer Netherlands: Dordrecht, 2000; pp 513−521.
(57) Elwi, T. A.; Al-Rizzo, H. M.; Rucker, D. G.; Dervishi, E.; Li, Z.; Biris, A. S. Multi-Walled Carbon Nanotube-Based RF Antennas. *Nanotechnology* **2010**, *21*, 045301.
(58) Elwi, T. A.; Rucker, D. G.; Al-Rizzo, H. M.; Khaleel, H. R.; Dervishi, E.; Biris, A. S. A Dual-Frequency Wearable MWCNT Ink-Based Spiral Microstrip Antenna. *Nanotech 2010: Advanced Materials, CNTs, Particles, Films and Composites—Technical Proceedings of the 2010 NSTI Nanotechnology Conference and Expo, NSTI-Nanotech 2010*, 2010; Vol. *1*, pp 266−269.
(59) Rezaeieh, S. A.; Zamani, A.; Bialkowski, K. S.; Mahmoud, A.; Abbosh, A. M. Feasibility of Using Wideband Microwave System for Non-Invasive Detection and Monitoring of Pulmonary Oedema. *Sci. Rep.* **2015**, *5*, 1−11.
(60) El-Bahii, M. M. Antenna for Lung Cancer Detection Using Electric Properties of Lung Tissues. *GSJ* **2021**, *9*, 1327−1332.
(61) Aydin, E. A. A Novel Flexible Microstrip Patch Antenna with Different Conductive Materials For Telemedicine and Mobile Biomedical Imaging Systems. *Mapping Intimacies* **2021**, DOI: 10.21203/rs.3.rs-664932/v1.
(62) Abdelhamid, M. M.; Allam, A. M. Detection of Lung Cancer Using Ultra Wide Band Antenna. *2016 Loughborough Antennas & Propagation Conference (LAPC)*; IEEE, 2016; pp 7−11.
(63) Journal, I. Design and Analysis of Microstrip Patch Antenna for Different Applications. *Int. J. Sci. Res.* **2017**, *6*, 421−424.
(64) Song, R.; Zhao, X.; Wang, Z.; Fu, H.; Han, K.; Qian, W.; Wang, S.; Shen, J.; Mao, B.; He, D. Sandwiched Graphene Clad Laminate: A Binder-Free Flexible Printed Circuit Board for 5G Antenna Application. *Adv. Eng. Mater.* **2020**, *22*, 2000451.
(65) Ramli, M. R.; Ibrahim, S.; Ahmad, Z.; Abidin, I. S. Z.; Ain, M. F. Stretchable Conductive Ink Based on Polysiloxane-Silver Composite and Its Application as a Frequency Reconfigurable Patch Antenna for Wearable Electronics. *ACS Appl. Mater. Interfaces* **2019**, *11*, 28033−28042.

https://doi.org/10.1021/acsomega.2c02550
ACS Omega 2022, 7, 28265−28274